Journal of Marine Research, 74, 175–199, 2016

Mechanisms controlling vertical variability of subsurface chlorophyll maxima in a mode-water eddy

by Qian P. Li[1,2] and Dennis A. Hansell[3]

ABSTRACT

An intense subsurface chlorophyll enhancement was found repeatedly within the core of a mode-water eddy during a 2-month period. Two controls on chlorophyll concentrations in this deep chlorophyll maximum (DCM) layer are noted: chlorophyll concentration is controlled by nutrients at low nutrient concentrations and by light when nutrients are saturating. To synthesize these results, a simple one-dimensional nutrient-phytoplankton model is developed by including the effects of phytoplankton self-shading for light attenuation, depth-dependent phytoplankton specific loss, and density-associated nutrient fluctuation in the deep layer. The model is parameterized using eddy data including not only vertical diffusivity, sinking velocity, and chlorophyll-to-carbon ratios, but also rates of phytoplankton growth and nutrient regeneration. Our results suggest that the observed DCM variability is controlled by nutrient-light interaction leading to a change of phytoplankton physiology and hence vertical enrichment of chlorophyll within the core of the stratified eddy. Further theoretical analyses indicate that variation of nutrient and light availability in the DCM layer of the eddy core is largely driven by change of the vertical nutrient fluxes as a result of isopycnal motions in the deep layer, which is also subject to influences by processes including vertical mixing, particle sinking, and nutrient regeneration.

Keywords: Deep chlorophyll maximum, mesoscale eddy, vertical nutrient fluxes, phytoplankton sinking, nutrient regeneration, biophysical modelling

1. Introduction

The subsurface maximum of phytoplankton chlorophyll typically observed near the base of the euphotic zone is undetectable by remote sensing (Probyn, Mitchell-Innes, and Searson 1995) yet important for primary production (Goericke and Welschmeyer 1998), supported by the diffusive flux of nutrients from below (Cullen 2015). The magnitude of the subsurface biomass maximum (SBM) depends more on diffusion and sinking than on phytoplankton growth and loss, whereas the depth of the maximum is influenced by all these factors,

1. State Key Laboratory of Tropical Oceanography, South China Sea Institute of Oceanology, Chinese Academy of Sciences, 164 Xingang Road, Guangzhou, 510301, China.
2. Corresponding author: ***e-mail: qianli@scsio.ac.cn***
3. Department of Ocean Sciences, Rosenstiel School of Marine and Atmospheric Science, University of Miami, 4600 Rickenbacker Causeway, Miami, FL 33149, USA.

according to a one-dimensional (1D) nutrient-phytoplankton model (Hodges and Rudnick 2004). Further theoretical investigation suggests that reduced turbulent mixing will cause chaotic oscillations in the SBM, thus influencing primary production and phytoplankton species composition (Huisman et al. 2006). Beckmann and Hense (2007) extend the work by including detritus in the model and distinguishing between the factors determining the depth and shape of SBM and factors affecting vertically integrated primary production. The formation of a deep chlorophyll maximum (DCM), a result of elevation in cellular chlorophyll content (Cullen 1982, 2015), is more complicated than a biomass maximum (Fennel and Boss 2003) as the chlorophyll-to-biomass ratio of phytoplankton varies substantially at depth in response to varying nutrient concentrations, light levels and temperature (Geider MacIntyre, and Kana 1997; Li et al. 2010). Mechanisms for DCM variability in the highly stratified open ocean, however, are still inadequately understood, because of the internal complexity of the DCM community and the external dynamics of physical forcing (Strass 1992; Letelier et al. 2004; Li et al. 2012; Cullen 2015).

A subsurface chlorophyll bloom in a mode-water eddy was observed in the Sargasso Sea near Bermuda during the summer of 2005 (McGillicuddy et al. 2007). Consistent with the small-scale characteristics of the chlorophyll bloom when rotating around the eddy center, as revealed by a video plankton recorder (Bibby et al. 2008), repeated sampling at the eddy center captured large variations in the depths and amplitude of DCMs. The intensity of the subsurface chlorophyll patch, however, had been relatively stable, with similar high concentrations regularly found within the eddy core (the area covered by a radius of 10 km around the eddy center based on Acoustic Doppler Current Profiler (ADCP) measurements) during the entire period of observations. The chlorophyll bloom, associated with a vertical diffusivity of $0.35 \pm 0.05 \times 10^{-4}$ m^2 s^{-1} based on a tracer-injection technique (Ledwell, McGillicuddy, and Anderson 2008), was sampled for about 2 months without noticeable change in vertically integrated zooplankton biomass (Goldthwait and Steinberg 2008) or in export fluxes of particles (Buesseler et al. 2008), suggesting that it might be in a relatively stable phase. The isolated nature of the mode-water eddy, with stable temperature/salinity (T/S) properties in the core provides an opportunity to investigate the mechanisms controlling DCM variability, away from highly perturbed surrounding waters with complex T/S characteristics resulting from enhanced physical mixing at the eddy edge (Li et al. 2008).

In this article, we investigate the interactions among nutrients, light, and chlorophyll in controlling the DCM located in the core of the eddy, using field data analyses and a simple nutrient-phytoplankton model coupling vertical physics and biology. The model takes into account the effects of phytoplankton self-shading for light attenuation, depth-dependent phytoplankton specific loss, and density-associated nutrient fluctuation in the deep layer, which have been neglected in many previous studies. Parameterized by various field data collected within the eddy, the model is used to explore the mechanisms of isopycnal motion, turbulent diffusion, particle sinking, and nutrient regeneration in controlling the intense subsurface chlorophyll maxima in the eddy core. The rest of the article is organized

as descriptions of materials and methods in Section 2, the model development and parameterizations in Section 3, major observational and model results in Section 4, the model and data comparison in Section 5, the discussion of physical and biological interaction in the DCM layer in Section 6, and conclusions from the major findings in Section 7.

2. Materials and methods

a. Study area and hydrography

The mode-water eddy was located in the Sargasso Sea near Bermuda (~66.5° W, 30.5° N). It was identified and tracked with satellite altimetry (McGillicuddy et al. 2007). The physical center of the eddy was determined from shipboard ADCP measurements. Field investigations were performed during two cruises aboard R/V *Oceanus* from June 12 to August 25, 2005. Comprehensive hydrographic and biogeochemical surveys were conducted immediately after the physical center of the eddy was located. Repeat samplings were made in the eddy core throughout the surveys. High-resolution hydrographic data from the upper water column were collected using a SeaBird SBE 9/11 conductivity-temperature-depth (CTD) with internal conductivity, temperature, oxygen, and fluorescence sensors. Discrete water samples were collected at the depths of 0, 20, 40, 60, 70, 80, 90, 100, 110, 120, 140, 200, 300, 500, and 700 m using a 24-place CTD-mounted rosette sampler with 12 L PVC Niskin bottles.

b. Measurements of nutrients, chlorophyll, and light

Nutrient samples were taken after inline filtration through 0.8 μm Nuclepore filters from Niskin bottles and measured at sea within 30 min of sampling. Nitrate plus nitrite (DNN) and dissolved inorganic phosphate (DIP) were measured simultaneously by a highly sensitive flow-injection system with long-path-cell spectrophotometry (Li and Hansell 2008). The detection limit was 2 nM for DNN, 0.5 nM for nitrite, and 1 nM for phosphate. Each sample was analyzed up to six times with a coefficient of variation <5%. Chlorophyll-*a* (Chl-*a*) concentrations were estimated from CTD fluorescence after calibration with the extracted Chl-*a* measurements by a Turner fluorometer (10-AU) in the field. Photosynthetically active radiation (PAR) was measured by a CTD-mounted PAR sensor and calibrated by measurements from optical probes. Because of daily variations of surface PAR, we use the daily mean PAR to interpret our data, which is the product of the percentage of light penetration and the average daily surface PAR.

c. Measurements of particulate organic carbon and nitrogen, growth rates, and chlorophyll-to-carbon ratios

For suspended particulate organic carbon (POC) and nitrogen (PON), 2 L of water collected in polypropylene bottles was filtered onto precombusted 25 mm Whatman GF/F filters, which were then wrapped in precombusted aluminum foil and stored frozen until

analysis by a control elemental analyzer. Primary production (mgC m^{-3} d^{-1}) data are taken from published results (McGillicuddy et al. 2007), determined by the ^{14}C incubation method employed at the Bermuda Atlantic Time-series Study (BATS). Growth rates of phytoplankton were estimated by dividing the primary production rates by the concentrations of POC in the same water. Because we did not have the carbon biomass data for phytoplankton, bulk cellular Chl-*a*-to-carbon ratios were approximated by dividing the Chl-*a* concentrations by the concentrations of POC. As POC contains particles other than phytoplankton, the Chl-*a*-to-carbon ratios are underestimates.

d. Nutrient-utilization experiments at the DCM

Water at a depth of ~110 m (DCM) for a station at the eddy center was collected by Niskin bottle (initial Chl-*a* of ~1.8 mg m^{-3}) and delivered to an acid-clean Nalgene carboy. Subsamples of water were transferred to 1,000 mL Nalgene PETG bottles. A nutrient-saturated treatment included adding nitrate and phosphate in combination to obtain final concentrations of ~3.2 μM of $NaNO_3$ and ~0.2 μM of KH_2PO_4. The bottles were sealed by wrapping with Parafilm and electrical tape before being placed in an on-deck incubation chamber equipped with a flow-through seawater system. The incubator was shaded to simulate the averaged daily light level at the DCM (~5 μE m^{-2} s^{-1}). Duplicate samples were incubated continuously for 3 days. A water sample (10 mL) was taken each day at noon and frozen immediately for nutrient analyses. These samples were determined in the lab by the Flow Injection Analysis-spectrophotometry method described previously. The theory for retrieving phytoplankton loss rates from incubation experiments will be described in Section 3c.

3. Model development and parameterizations

a. Theory for the interactions of Chl-a, light, and nutrients in the DCM

We develop a 1-D nutrient-phytoplankton model to diagnose the field observations and to predict DCM variability in the eddy core. We define P as phytoplankton nitrogen biomass, N as nitrate concentration, μ and R as the specific rates of phytoplankton growth and loss (death, grazing, etc.), k_z and w_s as the vertical diffusivity and sinking velocity. A list of model parameters is provided in Table 1.

When neglecting horizontal and vertical advection, the rate of phytoplankton change is controlled by the net growth, diffusion, and sinking of phytoplankton (e.g., Fennel and Boss 2003), which is expressed as follows:

$$\frac{dP}{dt} = (\mu - R) \cdot P + k_z \frac{d^2 P}{dz^2} - w_s \frac{dP}{dz}. \quad (1)$$

Both k_z and w_s vary with depth, but for simplification, they are assumed constant. The general diffusive behavior of phytoplankton is considered and is assumed equal to the diffusion coefficient of nitrate. The vertical migration of diatoms may be important for

Table 1. List of parameters for model equations. PAR, photosynthetically active radiation.

Symbol	Parameter	Value	Units	Source
w_s	Sinking velocity of particles	0.2	m d^{-1}	Buesseler et al. (2008)
k_z	Vertical eddy diffusivity	3.5×10^{-5}	m^2 s^{-1}	Ledwell, McGillicuddy, and Anderson (2008)
R_0	Maximal phytoplankton loss rate	0.34	d^{-1}	Data
μ_{max}	Maximal growth rate at 0°C	1.0	d^{-1}	Data
c	Temperature coefficient	0.07	$°C^{-1}$	Eppley (1972)
K_n	Half-saturation constant for nitrate uptake	0.6	mmolN m^{-3}	Data
K_{sw}	Light attenuation attributable to seawater	0.035	m^{-1}	Data
K_{ph}	Light attenuation attributable to phytoplankton	0.086	$(\text{mmolN m}^{-2})^{-1}$	Data
θ_m	Maximal chlorophyll-to-carbon ratio	0.030	gChl $(\text{gC})^{-1}$	Data
α^{chl}	Chlorophyll-specific initial slope of P-I curve	4.5	gC $(\text{gChl})^{-1}(\text{W m}^{-2}\ \text{d})^{-1}$	Mackey et al. (2008)
α	Initial slope of P-I curve	0.14	$(\text{W m}^{-2}\ \text{d})^{-1}$	Data
I_0	Averaged daily cloud-corrected surface PAR during July and August	143	W m^{-2}	Data
P_0	Phytoplankton biomass at surface	0.05	mmolN m^{-3}	Data
N_1	Nitrate concentration at 200 m		mmolN m^{-3}	

diatom-dominant systems (Villareal et al. 1999) but is neglected here, as diatoms were only ~20% of the total chlorophyll (McGillicuddy et al. 2007).

If phytoplankton losses are assumed to be fully regenerated back to nitrate (i.e., the loss rate is equal to the regeneration rate; Hodges and Rudnick 2004), we have

$$\frac{dN}{dt} = -(\mu - R) \cdot P + k_z \frac{d^2N}{dz^2}. \tag{2}$$

We neglect nutrient regeneration by detritus and zooplankton, which allow investigation of major processes influencing the vertical phytoplankton distribution in general. We also assume the loss of organic nitrogen is instantaneously remineralized to nitrate. The validity of equation (2) will be addressed in Section 5 when it is replaced by a data-regression equation.

A typical stable water structure, describing the balance of phytoplankton growth and vertical nutrient flux, has been proposed as a framework for understanding how interactions of nutrient flux and photon flux affect the vertical distribution of phytoplankton (Cullen 2015). We chose to explore the steady-state solution to the nutrient-phytoplankton model, as the chlorophyll bloom is a relatively stable feature rotating around the eddy center within the eddy core from a three-dimensional (3-D) point of view (see the second paragraph of Section 1). In fact, we are focused on a very thin layer of the eddy core as its horizontal scale (20 km in diameter) is more than 100 times the vertical scale of the euphotic zone (200 m).

In steady state ($dP/dt = 0$ and $dN/dt = 0$), equations (1) and (2) can be reorganized as second-order ordinary differential equations (ODEs)

$$\frac{d^2P}{dz^2} = \frac{w_s}{k_z}\frac{dP}{dz} - \frac{(\mu - R)}{k_z} \cdot P \tag{3}$$

and

$$\frac{d^2N}{dz^2} = \frac{(\mu - R)}{k_z} \cdot P. \tag{4}$$

Combining equations (3) and (4) and integrating over depth, assuming no surface net flux $(dN/dz)_0 + (dP/dz)_0 - (w_s/k_z)P_0 = 0$ with P_0 the surface biomass, we have

$$\frac{dN}{dz} + \frac{dP}{dz} = \frac{w_s}{k_z} \cdot P. \tag{5}$$

This equation states that the diffusive fluxes of nitrate should be balanced by the sinking fluxes of phytoplankton at steady state.

Our model thus includes a second-order ODE for phytoplankton (equation 3) and a first-order ODE for nitrate (equation 5). Numerical solution to a system of two ODEs can be acquired with the boundary conditions: $dP/dz = 0$ and $P = P_0$ at $z = 0$ (no phytoplankton flux through the surface), together with $P = 0$ and $N = N_1$ at $z = 200$ m

(no phytoplankton in the deep layer). We also assume $N = 0$ at the surface in order to get the vertical P integration. The ODEs are solved using MATLAB solver BVP5C for boundary value problems (e.g., Shampine and Reichelt 1997) with a vertical resolution of 0.5 m per step. Note that both μ and R in equation (3) should be computed before solving the system.

Applying a version of the growth equation adapted from Li et al. (2010) without photoinhibition and silicate limitation to the eddy core, we have

$$\mu = \mu_{\max} \cdot e^{cT} \cdot \frac{N}{K_n + N} \cdot \left[1 - \exp\left(-\frac{\alpha \cdot I}{\mu_{\max}}\right)\right], \tag{6}$$

where K_n is the half-saturation constant for nitrate uptake; $\mu_{\max}$ is the maximal growth rate at 0°C; c is the temperature-dependence coefficient; α is the initial slope of the photosynthesis-irradiance ($P - I$) curve; and I is the PAR (in W m^{-2}), which is attenuated with depth according to Lambert-Beer's law:

$$I = I_0 \cdot \exp\left(-K_{sw} \cdot z - K_{ph} \cdot \int_0^z P \cdot dz\right). \tag{7}$$

In equation (7), K_{sw} and K_{ph} are the attenuation coefficients because of seawater and phytoplankton, respectively, and I_0 is the daily averaged cloud-corrected surface PAR and remains constant in time.

We have included the integrated effect of phytoplankton self-shading on light attenuation, which is neglected in many previous models (e.g., Fennel and Boss 2003; Hodges and Rudnick 2004). Some studies (e.g., Beckmann and Hense 2007) consider the self-shading of phytoplankton but do not integrate them through the water column, which will lead to substantial underestimates of light attenuation below the DCM. The integral in equation (7), however, introduces a nonlocal term to the differential equations, which is computationally costly as it requires implicit integration (Huisman et al. 2006). We calculate the integral from equation (5) by $\int_0^z P \cdot dz = k_z / w_s \cdot (P + N - P_0)$ assuming negligible nitrate at the surface.

We allow the specific loss rate R to vary with P as

$$R = R_0 \cdot \left[1 - \exp\left(-\frac{P}{P_{\text{avg}}}\right)\right], \tag{8}$$

where R_0 is the maximal loss rate (d^{-1}), and P_{avg} is the average phytoplankton biomass (mmolN m^{-3}) estimated by $P_{\text{avg}} = (1/200) \int_0^{200} P \cdot dz$. Here, we have neglected the complex food web and microbial loop dynamics. Equation (8) is identical to the classical Ivlev grazing function if we assume a vertically constant ratio of heterotroph to autotroph, which is relatively constant in the oligotrophic gyre (Calvo-Diaz et al. 2011) because of tight coupling between phytoplankton growth and grazing (Gasol, del Giorgio, and Duarte 1997). With equation (8), R will show a subsurface maximum at the depth of maximal biomass, consistent with the observations of vertically elevated abundances of bacteria and zooplankton there (Ewart et al. 2008; Goldthwait and Steinberg 2008). Previous studies generally

assume a vertically constant phytoplankton loss rate ($R = R_0$) (e.g., Beckmann and Hense 2007; Denaro et al. 2013), resulting in higher nitrate at depths below the DCM. This higher nitrate is because of fast decrease of growth rate by light limitation, leading to a large negative net growth rate ($\mu - R << 0$) when R is a constant. In this case, there is too much remineralization below the DCM and thus extra nitrate released to seawater.

The model Chl-*a* is calculated by multiplying phytoplankton nitrogen biomass by the cellular Chl-*a*-to-nitrogen ratio γ (units: μgChl μgN^{-1}). Assuming a Redfield N:C ratio, γ is related to the Chl-*a*-to-carbon ratio θ (units: μgChl μgC^{-1}) by $\gamma = 5.679\theta$. For balanced growth, θ can be predicted by a nonlinear equation describing phytoplankton acclimation to varying nutrient, light, and temperature (Geider, MacIntyre, and Kana 1997; Li et al. 2010):

$$(\boldsymbol{\theta}/\boldsymbol{\theta}_m)^2 = \frac{1 - \exp(-\omega\boldsymbol{\theta}/\boldsymbol{\theta}_m)}{\omega}, \tag{9}$$

where θ_m is the maximal Chl-*a*-to-carbon ratio, and ω is given by $\omega = \theta_m \alpha^{\mathrm{chl}} I / P_{\max}$ with α^{chl} and $P_{\max}$ representing the Chl-*a*-normalized initial slope and the maximum carbon-specific photosynthetic rate of the P-I curve (Geider, MacIntyre, and Kana 1997). We integrate the model from the surface to 200 m to predict the profiles of P, N, and I, from which we compute the vertical chlorophyll distribution.

A constant nitrate at the deep boundary (N_1) is often assumed in previous models of DCM or SBM (e.g., Fennel and Boss 2003; Huisman et al. 2006; Denaro et al. 2013), which, however, will not hold for the eddy here because of changes of nitrate at 200 m in the eddy core. By affecting the vertical nutrient flux, nutrient variations in the source water for vertical mixing could influence the vertical structure of phytoplankton (Beckmann and Hense 2007). On the other hand, the 1-D approach so far does not consider vertical advection, such as Ekman pumping, which drives isopycnal motions particularly at the deeper layer (no vertical velocity at the surface because of water continuity). As the deep boundary layer is high nutrient ($N = N_1$) but low biomass ($P = 0$), vertical advection will have a much larger effect on equation (2) than on equation (1). One way to modify nutrient equation (2) is by including vertical velocity, which, however, is difficult to quantify because of the small size of the chlorophyll patch and because of the large variation of velocity inferred from strong density displacements in the deep layer of the eddy core. To represent the density-associated variation of nitrate below euphotic zone, we allow the model N_1 to vary between 0.1 and 4 mmolN m^{-3}, in line with the observed range of nitrate change at 200 m. The fluctuation of N_1 is driven by isopycnal motion, as nitrate is tightly correlated with density for waters below 200 m in the eddy core (Li and Hansell 2008). A system with varying N_1 at 200 m will therefore give information on the effect of isopycnal motion on nutrient fluxes and phytoplankton dynamics.

b. Parameterization of DCM model with field data

The 1-D model is parameterized using field data including vertical diffusivity, sinking velocity, growth rate, nutrient regeneration, and Chl-*a*-to-carbon ratio. Tracer injection

experiments in the DCM of the eddy core suggest a relatively small diffusivity (k_z) of $0.35 \pm 0.05 \times 10^{-4}$ m^2 s^{-1} (Ledwell, McGillicuddy, and Anderson 2008). A mean sinking velocity (w_s) of 0.2 ± 0.04 m d^{-1} for phytoplankton in the DCM is estimated from sediment trap measurements when the POC flux of 12.4 ± 0.2 mgC m^{-2} d^{-1} is divided by the POC concentration of 62 ± 11 mgC m^{-3} in August 2005 (McGillicuddy et al. 2007). This velocity is comparable with observations at BATS during July–August 2005.

We estimate a seawater attenuation (K_{sw}) of 0.035 m^{-1} and a phytoplankton attenuation (K_{ph}) of 0.086 (mmolN m^{-2})$^{-1}$ based on fitting of equation (7) to PAR and PON data in the eddy, in agreement with BATS measurements (Siegel et al. 2001). Daily averaged PAR just beneath the sea surface (I_0) during the cruises was ~142 W m^{-2}, which is consistent with BATS data in summer (Goericke and Welschmeyer 1998). In the open ocean, the half-saturation constant (K_n) of phytoplankton nitrate uptake is higher in the DCM layer (>0.5 μmolN L^{-1}) than in the mixed layer (<0.1 μmolN L^{-1}) (Probyn, Mitchell-Innes, and Searson 1995; Weston et al. 2005). We chose a K_n of 0.6 μmolN L^{-1} based on the observed shifting of nutrient control to light control of chlorophyll at this level.

When fitting data of growth rate (together with Chl-*a*, nitrate, and temperature) into equation (6), we estimate a maximal growth rate (μ_{max}) of 1.0 d^{-1} and an initial slope of the *P-I* curve (α) of 0.14 (W m^{-2}d)$^{-1}$ by minimizing the sum of the squared residuals of the modeled and observed growth rates (Li et al. 2010). The mean α^{chl}, estimated from α after dividing by θ, is ~4.5 gC (gChl)$^{-1}$(W m^{-2}d)$^{-1}$ for the DCM, which agrees well with previous results of DCM near Bermuda from photosynthesis-irradiance experiments (Mackey et al. 2008). For simplification, the temperature effect on phytoplankton growth is neglected in the model by assuming a vertically constant value of 19.3°C.

c. *Estimation of the phytoplankton loss rate from nutrient consumption experiments*

In an incubation vessel, where physical forcing (diffusion and sinking) is neglected, we have from equations (1) and (2):

$$\frac{dP}{dt} = (\mu - R) \cdot P, \tag{10}$$

$$\frac{dN}{dt} = -(\mu - R) \cdot P. \tag{11}$$

From equation (6), we have the nutrient-saturated growth rate (μ_n) as

$$\mu_n = \mu_{max} e^{cT} \left[1 - \exp\left(-\frac{\alpha I}{\mu_{max}}\right)\right]. \tag{12}$$

As the amplitude of daily irradiance change was very low during the incubation, growth rate under such fluctuating light (~1% surface PAR) can be mostly the same as under constant light of the same averaged irradiance (Litchman 2000). Therefore, μ_n can be assumed constant in the incubation when the daily mean irradiance and temperature are

unvaried. Because phytoplankton Chl-*a* concentrations during the incubations were high, R could be assumed saturated and thus a constant as well ($R = R_0$).

The solution to equations (10) and (11), when μ and R are constant ($\mu = \mu_n$ and $R = R_0$), is

$$P = P_i \cdot e^{\lambda \cdot t} \tag{13}$$

$$N = C_i - P_i e^{\lambda \cdot t}, \tag{14}$$

where P_i and C_i are initial concentrations of phytoplankton nitrogen and total nitrogen before incubations, and λ is the net growth rate ($\mu_n - R_0$). Fitting of equation (14) to the experimental data, we can estimate λ and the loss rate $R_0 = \mu_n - \lambda$.

4. Results of observations and models

*a. Structure of density and Chl-*a *in the warm-core eddy*

The eddy was of a mode-water type, described as 18°C mode water captured in the subsurface eddy core. Figure 1 shows the 3-D depth structure of two of this eddy's isopycnal surfaces: $\sigma_\theta = 26.26$ and $\sigma_\theta = 26.7$, with color representing the concentrations of Chl-*a* on the upper surface. Doming of the upper thermocline ($\sigma_\theta = 26.26$) and depression of the deeper layer ($\sigma_\theta = 26.7$) is apparent (Fig. 1), creating a vertical divergence characteristic of mode-water eddies (Li and Hansell 2008). There is significant submesoscale variability for the depth of $\sigma_\theta = 26.26$ in the vicinity of the eddy center. High Chl-*a* concentrations are mostly located within the eddy core, where upward heaving of isopycnals is found, compared with the periphery of the mode-water eddy (Fig. 1). The Chl-*a* distributions for all stations within the eddy core are shown in Figure 2. Given the sharply defined DCM layers in the water column (<20 m in vertical extent), continuous CTD Chl-*a* fluorescence data are used to map the DCM depths and to precisely calculate the DCM concentrations. It is clear that maximal chlorophyll concentrations in the DCM vary substantially in the eddy core, from <0.5 mg m^{-3} to >3.5 mg m^{-3} (Fig. 1).

b. Depth of the DCM and nitracline within the eddy

Though there is substantial variability found in the DCM depths (Fig. 2a), CTD data clearly show the constraint of density on the vertical position of DCM layer, as all DCMs in the eddy center fall on the same isopycnal of $\sigma_\theta \sim 26.26$ (Fig. 2b). The result indicates that variations in the depths of DCM in the eddy core are controlled by vertical motions of the water column, perhaps through controls on isopycnal heaving by Ekman pumping (e.g., Li et al. 2015). Figure 3 shows the relationship between the depths of the DCM and nitracline for three stations near the eddy center. These three stations are within 5 km of the eddy core. The depths of the DCMs are substantially different among these three stations (Fig. 3a) with the shallowest DCM at ~80 m and the deepest at ~110 m. The nitracline follows the depth of the DCM for each station (Fig. 3a and b), but the positions of the DCM and

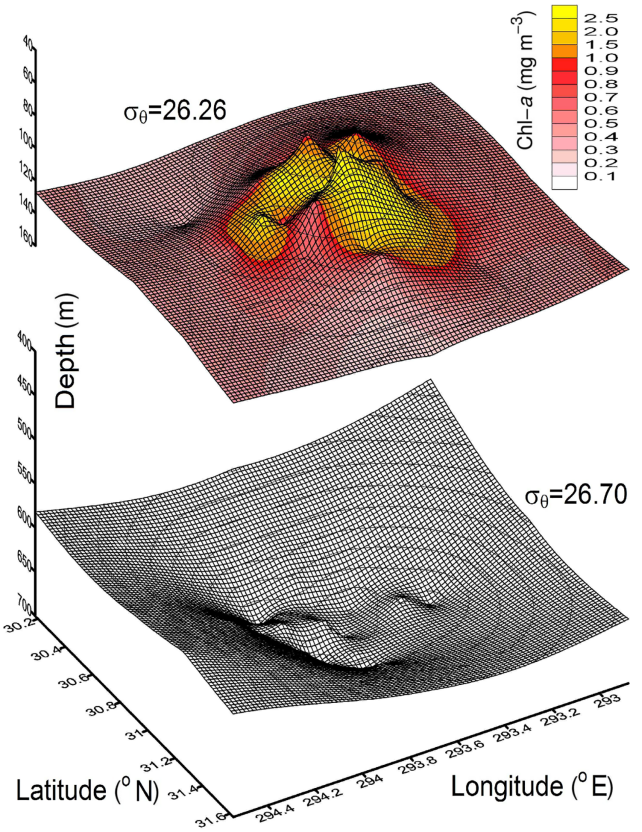

Figure 1. Structure of two density surfaces in a mesoscale eddy. The shallow isopycnal ($\sigma_\theta = 26.26$) marked the deep chlorophyll maximum in the eddy center. A deeper isopycnal of $\sigma_\theta = 26.7$ demonstrates the anticyclonic nature of the eddy (deepening of the surface at eddy center). Concentrations of Chl-*a* ($\mu g\ L^{-1}$) were contoured on the isopycnal surface of $\sigma_\theta = 26.26$. Note: These are not synoptic observations; the survey took 4 days with positions of the stations adjusted according to their distances from the eddy center. Chl-*a*, chlorophyll-*a*.

nitraclines for these three stations are almost identical when plotted on density (Fig. 3c and d), showing that they lie on the same isopycnal surface.

c. Nutrients and light at the DCMs

Large variabilities of Chl-*a* (0.48–3.57 mg m^{-3}), daily mean PAR (0.71–3.75 W m^{-2}), DNN (0.029–0.799 mmol m^{-3}), and DIP (0.008–0.032 mmol m^{-3}) were found in the DCMs within the eddy core, though their temperatures were relatively unvaried. Good correlations are seen for DNN ($r^2 = 0.85$, $P < 0.05$) and DIP ($r^2 = 0.82$, $P < 0.05$) with Chl-*a* in the DCMs at these stations (Fig. 4a and b). Although there is no overall

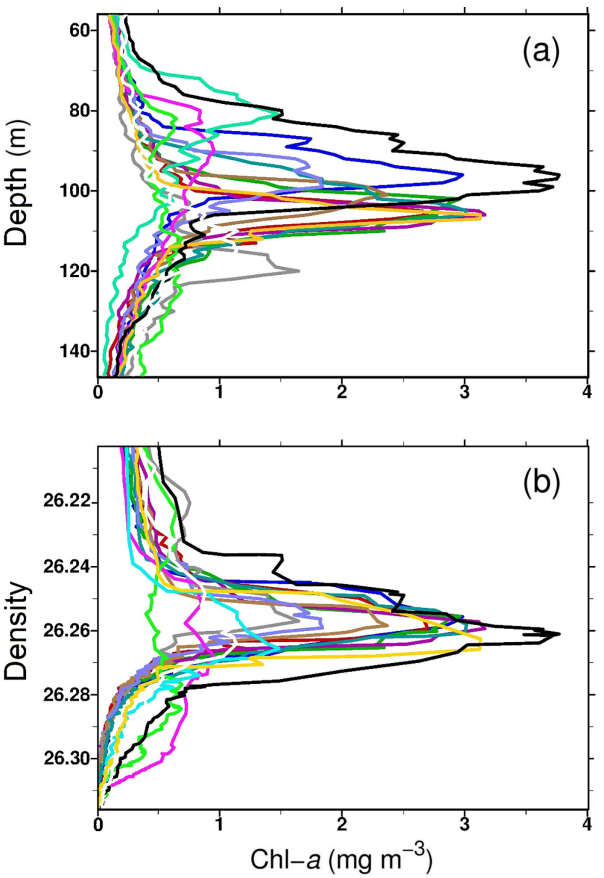

Figure 2. Vertical variability of conductivity-temperature-depth Chl-*a* in the eddy core at (a) depth and (b) density. Note that the depths of the deep chlorophyll maximum fall on the same density surface, $\sigma_\theta = 26.26$. Temperature/salinity analysis suggests that these profiles shared the same water masses. Chl-*a*, chlorophyll-*a*.

linear relationship between Chl-*a* and daily mean PAR (Fig. 4c), a strong linear correlation ($r^2 = 0.96$, $P < 0.05$) between Chl-*a* and PAR is found for stations with elevated Chl-*a* concentrations (>2.5 mg m^{-3}).

Stations with high DCM chlorophyll are always rotating around the eddy center within the core. When nutrient concentrations are low, DCM chlorophyll concentrations are well correlated with nitrate and phosphate concentrations in the eddy core (Fig. 4a and b), revealing nutrient control of the DCM community. However, for stations with elevated nutrients (DNN >0.5 mmol m^{-3} and DIP >0.025 mmol m^{-3} at DCM), concentrations of DCM Chl-*a* correlate not with nutrient concentrations ($r^2 = 0.02$, $P = 0.49$) but with

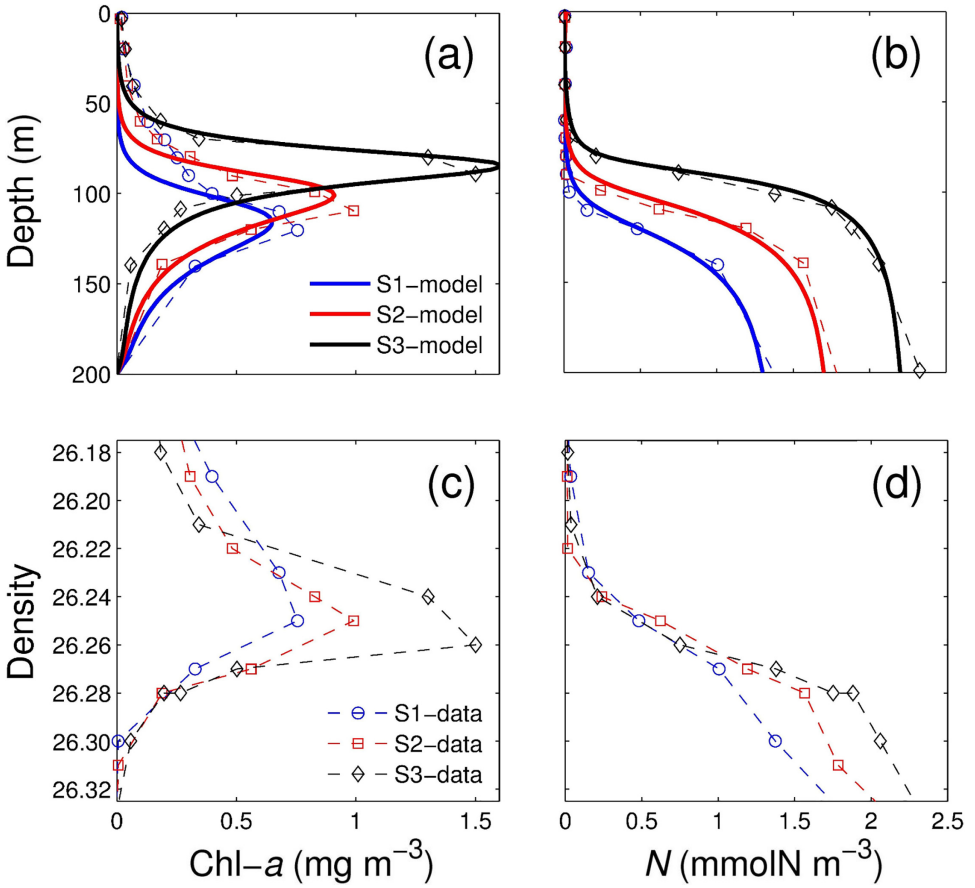

Figure 3. Vertical profiles of bottle chlorophyll-*a* (Chl-*a*) and nitrate (*N*) for three stations (S1, S2, and S3) at the eddy center: (a and b) plotted versus depth; (c and d) plotted versus density. Variability of deep chlorophyll maximum tracks the nitracline, but they all follow the $\sigma_\theta = 26.26$ isopycnal. Thick lines in panels (a) and (b) are model results for these stations with $N_1 = 1.3$ (blue), 1.7 (red), and 2.3 (black) mmolN m^{-3}.

light levels (<1% surface PAR; Fig. 4c), suggesting light control of DCM intensity. These results indicate that the high Chl-*a* patch is regulated by nutrient and light interaction.

d. Nutrient utilization in the DCM of the eddy core

Nitrate consumption with time (Fig. 5) during the incubation experiments was fitted into equation (14), estimating the net growth rate λ to be 0.49 ± 0.03 d^{-1} (similar rates were obtained from the phosphate experiments). From equation (12) with parameters in Table 1, the nutrient-saturated growth rate (μ_n) can be estimated as 0.83 ± 0.10 d^{-1} when incubated

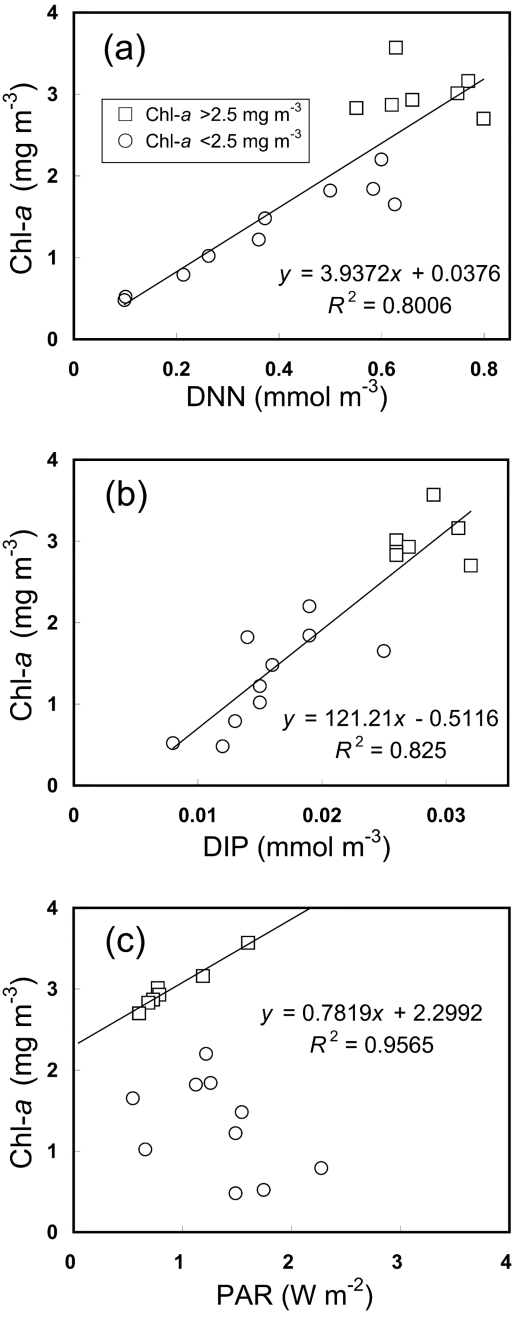

Figure 4. Relationships of chlorophyll-*a* (Chl-*a*) concentrations with (a) nitrate plus nitrite (DNN), (b) dissolved inorganic phosphate (DIP), and (c) daily mean photosynthetically active radiation (PAR) at the deep chlorophyll maxima of the eddy center. Square symbols are from stations with Chl-*a* >2.5 mg m^{-3}.

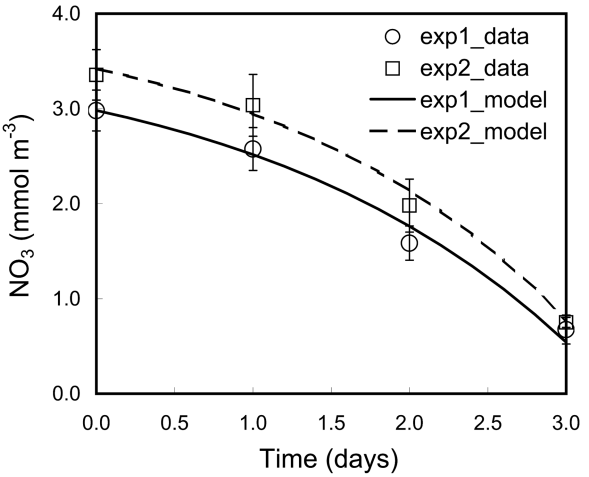

Figure 5. Nutrient utilization experimental results at the eddy center. Note: Water at the deep chlorophyll maximum was incubated under conditions resembling in situ daily mean photosynthetically active radiation and temperature apart from the nutrient saturation; these data were best fit by equation (15) to yield estimates of net growth rates (see text for details).

under daily averaged irradiance of $\sim$5 μE m^{-2} s^{-1} and temperatures of 26.5 $\pm$ 1.5°C. A maximal loss rate R_0 of 0.34 $\pm$ 0.13 d^{-1} is thus obtained by subtracting the net growth rate from the nutrient-saturated growth rate.

e. Variability of the model DCMs in the eddy core

Our 1-D model for the core of the mode-water eddy indicates that both physical and biological processes, including turbulent diffusion, particle sinking, and nutrient regeneration, contribute to the vertical location of DCMs (and consequently nitraclines) (Fig. 6). Generally, increased sinking (Fig. 6a3 and b3), reduced turbulent mixing (Fig. 6a4 and b4), and reduced nutrient regeneration (Fig. 6a2 and b2) will lead to a deeper nitracline and deeper Chl-*a* maximum. On the other hand, our model predicts that when rates of mixing, sinking, and maximal regeneration are constant, depths of the DCM and the nitracline will be determined by nitrate concentration at 200 m depth (N_1) (Fig. 6a5 and b5), which vary substantially because of isopycnal motion at 200 m below the euphotic zone, likely driven by processes such as Ekman pumping. This result is consistent with the observations of density constraints on the vertical positions of DCM and nitracline in the eddy core (Fig. 3).

In agreement with observations, the model predicts that Chl-*a* of the DCMs within the eddy core was simultaneously controlled by nutrient and light: Chl-*a* concentrations increased monotonically with nutrient concentrations until nutrients were saturating; they then increased with light levels (black lines in Fig. 7). In addition, the model predicts substantially lower Chl-*a* at higher light levels in the DCMs (Fig. 7b1), which is also consistent

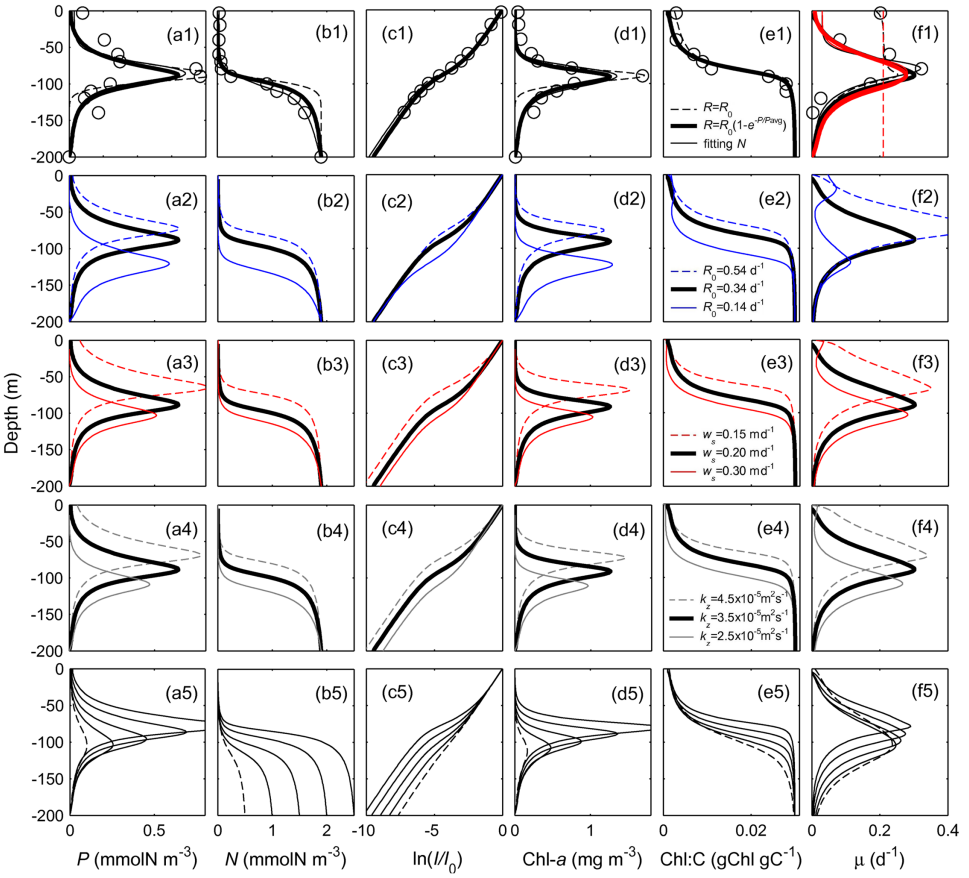

Figure 6. Vertical distributions of modeled variables including (a) phytoplankton, P; (b) nitrate, N; (c) light percentage, $\ln(I/I_0)$; (d) chlorophyll-a, Chl-a; (e) chlorophyll-to-carbon ratio, Chl:C; and (f) growth rate, μ, under different model conditions. The model conditions include the following: case 1 (a1–f1), $N_1 = 1.9$ mmolN m^{-3}, $R_0 = 0.34$ d^{-1}, $w_s = 0.2$ m d^{-1}, $k_z = 3.5 \times 10^{-5}$ m^{2}s^{-1}; case 2 (a2–f2), varying R_0 (0.14, 0.34, 0.54 d^{-1}) but others unvaried; case 3 (a3–f3), varying w_s (0.15, 0.2, 0.3 m d^{-1}); case 4 (a4–f4), varying k_z (2.5, 3.5, 4.5 $\times$ 10^{-5} m^2 s^{-1}); and case 5 (a5–f5), varying N_1 (0.5 to 2.5 mmolN m^{-3}). For a1–f1, the open circles are field data of a typical station at eddy center; three models are compared including a model with a constant loss rate (dotted lines), a model with a varying loss rate (thick solid lines), and a model with equation (2) being replaced by a regression fit of nitrate and depth (thin solid lines); red lines in F1 represent the vertical patterns of loss rate R for different models.

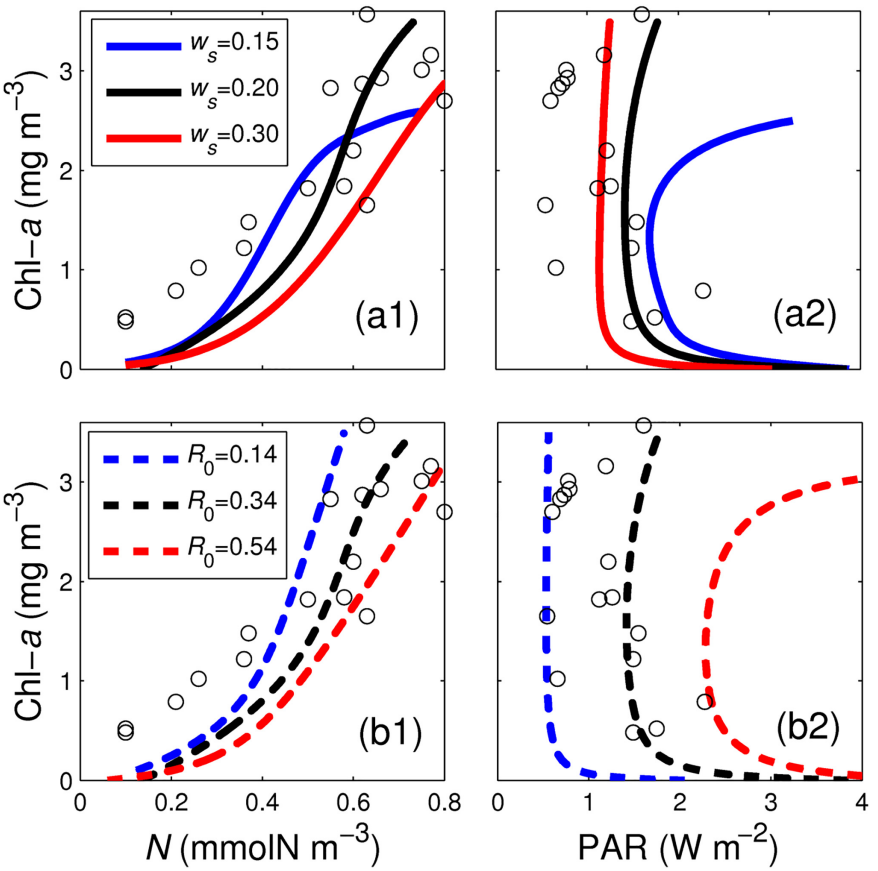

Figure 7. Relationships of nutrient and light with chlorophyll-*a* (Chl-*a*) in a modeled deep chlorophyll maximum (DCM) under (a1 and b1) different sinking velocities and (a2 and b2) different maximal regeneration rates. Open circles are observations in the DCMs of the eddy center with lines from model results. PAR, photosynthetically active radiation.

with observations (Fig. 4c). Further, model calculations suggest that lower Chl-*a* in higher-light environments at the DCM layer is a result of phytoplankton self-shading, as reduced phytoplankton biomass has led to enhanced light penetration (Fig. 6a5 and 6c5).

5. Model and data comparison

With a measured N_1 at 200 m, we can predict the vertical profiles of all variables by solving the parameterized model. Vertical patterns of chlorophyll and nutrient for three stations in the eddy core with large separations in DCM depths have been reasonably reproduced by the model (Fig. 3a and b). Model-data comparison is further examined for a well-sampled

station at the eddy center (Fig. 6a1–f1). At this station, the model accurately predicted not only the state variables including nutrients, phytoplankton, light, and Chl-*a*, but also the growth rate and Chl-*a*-to-carbon ratio. Generally, both phytoplankton biomass and Chl-*a* show subsurface maxima at the nitracline (Fig. 6a1, b1, and d1). It is worth mentioning that previous models with a constant loss rate ($R = R_0$) will overestimate nitrate (Fig. 6b1) but underestimate biomass and Chl-*a* (Fig. 6a1 and d1) for depths below the DCM. Light attenuates more quickly at depths where phytoplankton absorption increases (Fig. 6c1); thus, the depths where light attenuation is greatest correspond to the depths of maximal biomass (Fig. 6a1). The increase in Chl-*a*-to-carbon ratios from $\theta < 0.003$ at the surface to $\theta = \sim 0.03$ in the DCM (Fig. 6e1) is a result of phytoplankton photoacclimation to varying nutrient and light. Consistent with observations, the growth rate μ shows a maximum near the DCM and a fast decrease below (Fig. 6f1). These vertical patterns of Chl-*a*-to-carbon ratio and community growth rate are consistent with observations at BATS (Goericke and Welschmeyer 1998).

Biological processes affecting the vertical nitrate distribution, such as ammonium excretion, ammonium oxidization to nitrite, and nitrite oxidation to nitrate, may lead to vertical separations in the maxima of ammonium, nitrite, and chlorophyll (Lomas and Lipschultz 2006). To validate our nitrate equation, we replace equation (2), including its derived equations (4) and (5), with a data regression equation for a station in the eddy center (Fig. 6b1), while keeping other equations the same:

$$N = \begin{cases} 37.88 \times e^{-[(z-250.7)/29.22]^2} + 1.657 \times e^{-[(z-132)/34.65]^2} & \text{if } z \le 114 \\ 1.589 \times e^{0.001562\times(z-90)} - 1.311 \times e^{-0.05122\times(z-90)} & \text{if } z > 114 \end{cases}. \quad (15)$$

The new system is a single ODE (equation 3) with nitrate directly computed from depth by equation (15). The solution to a second-order ODE is found with two boundary conditions: $dP/dz = 0$ at $z = 0$ and $P = 0$ at $z = 200$ m. Vertical patterns of variables predicted by the single ODE model (thin black lines in Fig. 6a1–f1) are similar to the model of two ODEs (thick black lines in Fig. 6a1–f1, with $N_1 = 1.9$ mmolN m^{-3}). Both models show good agreement with observations at the station, which indicates that equation (2), though rather simple, can reasonably represent the vertical nitrate change in the eddy.

6. Discussion

a. Nutrient-light interaction controlling the magnitude of the subsurface chlorophyll maximum

Both observations and the model revealed a switching from nutrient to light control of chlorophyll concentrations with increasing nutrient concentrations in the DCM layer. Nutrient and light limitations of phytoplankton in the DCMs are further investigated using a ratio of growth sensitivity to nutrient and light, $r = (\partial\mu/\partial I)/(\partial\mu/\partial N) \cdot (K_I/K_n)$, which is an index comparing the sensitivity of growth to changes in nutrient (N/K_n) and light (I/K_I) resources (Cloern 1999). K_I is the half-saturation constant for light limitation,

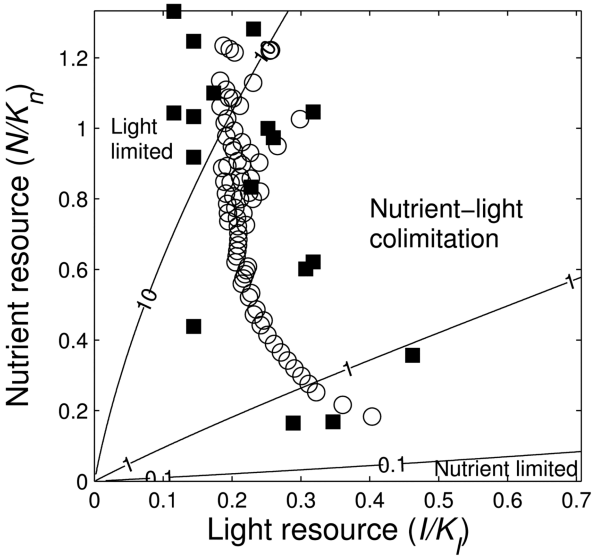

Figure 8. Light and nutrient-limitation of phytoplankton growth in the deep chlorophyll maxima of the eddy center from observation (squares) and model (open circles). Contour lines are the resource limitation map plotted as the ratio of growth rate sensitivity to light and nutrient based on parameters in Table 1; values >10 indicate light limitation, values <0.1 indicate nutrient limitation, and values = 0.1–10 indicate colimitation. K_I is the half-saturation constant for light limitation, and K_n is the half-saturation constant for nutrient uptake.

defined as the daily irradiance at which growth rate is half the maximum. Using growth equation (6), r can be expressed as

$$r = (1 + N/K_n) \cdot (N/K_n) \cdot \beta \cdot \frac{e^{-\beta \cdot (I/K_I)}}{1 - e^{-\beta \cdot (I/K_I)}}, \tag{16}$$

where $\beta = \alpha K_I/\mu_{\max}$ (parameter values in Table 1). Values of nutrient and light in the model DCMs with N_1 varying from 0.1 to 4 mmol m^{-3} are used to compute the modeled resource diagram (Fig. 8), which shows a reasonable agreement with the observation.

The resource diagram indicates a regime shift from nutrient and light colimitation ($10 > r > 0.1$) to light limitation ($r > 10$) of phytoplankton growth as nutrient increases in the DCM layer. Though nutrients are elevated in the DCM compared with the mixed layer, their concentrations (<0.8 mmol m^{-3} DNN and <0.04 mmol m^{-3} DIP) are still low enough to limit the growth of phytoplankton (Probyn, Mitchell-Innes, and Searson 1995). Nutrient limitation of the DCM community in the eddy core is also supported by measurements of photosynthetic physiology with a lower normalized variable fluorescence and a larger light-harvesting antenna size (σPSII), both of which were associated with reduced nutrient availability in the DCM layer (Bibby et al. 2008). For stations with higher

Chl-*a* (also high nutrient, $N > 0.6$ mmol m^{-3}), the resource index showed persistently strong light limitation. For these stations, changes in nutrient concentrations would have less effect on the growth and biomass accumulation of phytoplankton. For lower Chl-*a* regions where the index shows colimitation by nutrient and light availability, it is more likely that changes in nutrient input will lead to large phytoplankton responses. It is possible that phytoplankton in the DCM of the eddy core experience nonsaturating nutrients and light-limiting conditions similar to the spring phytoplankton bloom (Riegman 1998). In such an environment, primary production is driven by irradiance but constrained by nutrient limitation.

In the model DCMs, chlorophyll variability in response to nutrient-light interaction is a result of changing vertical nutrient flux induced by density-associated nitrate fluctuation at the deep boundary layer. This is because Chl-*a*, nitrate, and light are determined by N_1 when other factors including k_z, w_s, and R_0 remain constant (Fig. 6a5–f5). In fact, both model and observations suggest that phytoplankton growth is more sensitive to changes in nutrients than in light in the DCM, as nutrient resource varied by a much broader range (0.1–1.3) than the light resource (0.1–0.5). When the vertical nutrient flux is low (low N_1), slow growth of phytoplankton leads to a low nutrient uptake rate in the DCM to consume the supply (Fig. 6a5–f5). When the nutrient flux is high (higher N_1) but is still not nutrient-saturated in the DCM, phytoplankton will grow rapidly in response to the increased nutrient availability even at a low irradiance (because of high self-shading). When the flux is high enough to result in a nutrient-saturation of phytoplankton growth in the DCM, a higher new production rate is achieved by phytoplankton growing at a higher irradiance to balance the nutrient supply. In summary, a phytoplankton community will change its growth and uptake physiology to establish equilibrium between its nutrient demand and the vertical nutrient flux and thus a stable DCM in the water column.

b. Influences of vertical diffusion and sinking on nutrient-light interaction in DCMs within eddies

By changing the parameters of sinking velocity and vertical diffusivity in the model, we can address the impacts of sinking and diffusion on the nutrient-light interaction at the DCM layer. Our model predicts that reduced sinking velocity of phytoplankton will result in a saturation of Chl-*a* concentration at lower nitrate levels in the DCMs (Fig. 7a1). A change of sinking velocity does not show a large impact on the Chl-*a* and light relationship when the Chl-*a* concentration is low (<2 mg m^{-3}; Fig. 7b1), whereas the response of Chl-*a* to changing light levels varies significantly with the sinking velocity when Chl-*a* is high (>2 mg m^{-3}). In particular, the sensitivity of Chl-*a* to changes in light decreases substantially at lower sinking velocities, likely because reduced sinking would cause a phytoplankton maximum to be shallower, and thus phytoplankton are exposed to higher light but lower nutrient. The impact of increased diffusion on Chl-*a*-nutrient and Chl-*a*-light relationships is similar to that of reduced sinking velocity (data not shown). These results suggest that

vertical diffusion and sinking will affect subsurface Chl-*a* maxima by changing nutrient-light interaction in the DCMs.

Small variations in vertical diffusivity and sinking velocity are expected to have large impacts on the profiles of all the variables in the model. In particular, reduced sinking and enhanced diffusion can result in upward motions of nutrient and light profiles, which will lead to a shallower but stronger biomass/chlorophyll maximum. Light attenuation is strongly affected by vertical diffusion and sinking (Fig. 6c3 and c4) because of the shelf-shading effect of phytoplankton, in agreement with previous findings (e.g., Siegel et al. 1995). The model also predicts a deeper and lower growth rate maxima corresponding to an increased sinking velocity or a reduced diffusivity (Fig. 6f3 and f4), consistent with the contention of a lower phytoplankton production associated with higher export or lower nutrient flux. In reality, the sinking velocity of phytoplankton may vary when community structure changes. Also, the variation of turbulent diffusion is related to instabilities of the flows within the eddy, which will lead to density overturns and thus turbulent dissipations in the water column (Li et al. 2012).

The influences of vertical diffusion and sinking on the nutrient-light interaction in the DCM, however, should be largely constrained by the field observations of a relatively conservative diffusivity of $0.35 \pm 0.05 \times 10^{-4}$ m^2 s^{-1} and a sinking velocity of 0.2 ± 0.04 m d^{-1} in the DCM of the eddy core during the field observations, which are theoretically favorable for maintaining a stable deep biomass maximum (Huisman et al. 2006). This result is consistent with the observed long duration of the phytoplankton bloom in the eddy (McGillicuddy et al. 2007).

c. The role of nutrient regeneration for maintaining the subsurface chlorophyll maximum

Although biomass and Chl-*a* maximum are not significantly influenced by nutrient regeneration, our model predicts that an enhanced nutrient regeneration will lead to a shoaling of the nitracline, SBM, and DCM as more nutrients are released back to the seawater, relaxing the nutrient stress of the phytoplankton at higher light levels. In contrast to the effects of vertical diffusion and sinking, which change the entire light profile in the water column (Fig. 6c3 and c4), variations in nutrient regeneration show fewer impacts on the vertical light distribution except at the depths of the DCM (Fig. 6c2). It is also interesting to find that a change of nutrient regeneration does not influence the relationship between Chl-*a* and nitrate significantly (Fig. 7a2) but has large impacts on the relationship between Chl-*a* and light in the DCM (Fig. 7b2). Generally, the model predicts that reduced nutrient regeneration will lead to phytoplankton growth at lower irradiance in the DCM. It is quite possible that reduced regeneration has led to an increase of nutrient stress; thus, phytoplankton have to move downward to access the nutrients in the deeper layers, adapting to the lower light environment there.

Nutrient regeneration supports 84%–97% of primary production in the model DCM if we divide the regeneration rate by the growth rate there, leading to an f-ratio (the fraction

of total primary production fuelled by nitrate) of 0.03–0.16, which is comparable with the annual mean of 0.08-0.39 at BATS (Lipschultz 2001). In fact, new production by upward nitrate fluxes was ∼0.02 mmolN m^{-3} d^{-1} (Ledwell, McGillicuddy, and Anderson 2008), an order of magnitude lower than primary productivity of ∼0.2 mmolN m^{-3} d^{-1} in the DCM of the eddy center (McGillicuddy et al. 2007). The excess ^{234}Th below the DCM of the eddy core, however, suggested that 65% of the sinking particle flux was remineralized within 120–300 m (Buesseler et al. 2008). We should expect the model to overestimate regeneration as it implicitly includes losses from zooplankton grazing under the assumption of regeneration being equal to phytoplankton loss. Also, detritus such as fecal pellets, not immediately remineralized, will not contribute to regeneration on short timescales, which is neglected in the simple model. These processes potentially will result in a portion of phytoplankton loss not returning to nitrate. Therefore, the upward nutrient fluxes will have to be balanced by the sum of the sinking fluxes and the part of phytoplankton loss escaping from regeneration. This will lead to lower sinking fluxes and thus lower phytoplankton biomasses in the model.

7. Conclusions

In order to understand mechanisms controlling variability of DCM in the core of a mode-water eddy, a simple 1-D nutrient-phytoplankton model is developed by including the physiology of phytoplankton photoacclimation to directly predict chlorophyll concentration rather than assuming a constant chlorophyll-to-biomass ratio. The model simultaneously takes into account the effects of phytoplankton self-shading light attenuation, depth-dependent phytoplankton-specific loss, and density-associated nutrient fluctuation at the deep boundary layer. These processes are important for modeling nutrient and light interaction in controlling phytoplankton chlorophyll dynamics in DCM but have been generally neglected in many previous DCM models (Fennel and Boss 2003; Hodges and Rudnick 2004; Huisman et al. 2006; Beckmann and Hense 2007; Denaro et al. 2013). Parameterized by field data of the eddy, the model reasonably predicts not only the vertical patterns of phytoplankton biomass, Chl-*a*, nutrient, light, Chl-*a*-to-carbon ratio, and phytoplankton growth rates, but also the relationships among Chl-*a*, nutrient, and light in the DCM of the eddy core. Our findings suggest the shifting of resource stress of phytoplankton growth from nutrient control to light control in the DCM, which can be largely attributed to different vertical nutrient fluxes as a result of density-associated variations in nutrient concentration below the euphotic zone. The model also reveals important but distinct impacts of turbulent diffusion, vertical sinking, and nutrient regeneration on nutrient-light interaction in the DCM layer, contributing to vertical variability of Chl-*a* maxima in the eddy center.

It should be mentioned that the dynamics of nutrient-phytoplankton interaction within the core of the mode-water eddy are much more complicated than the simple model considered here. For example, our model has ignored factors such as depth variations of diffusivity and sinking velocity, community structure, horizontal advection, and zooplankton grazing,

which may affect our results. Also, the steady status assumption of the DCM may be violated under strong perturbations such as extremely heavy storms or hurricanes, which could break the balance between phytoplankton growth and vertical nutrient fluxes in the water column. In that case, temporal evolution of the DCM in response to a nutrient pulse would need to be addressed. Future study of DCM dynamics in isolated oligotrophic eddies may be improved by taking in account these processes in a more complex ecosystem model.

Acknowledgments. We thank Peter Franks for constructive comments on the manuscript. We also benefited from discussions with and comments from Paul Falkowski, Tom Bibby, Peter Ortner, and Dennis McGillicuddy. The modeling work was supported by an award from National 1000-Talent Recruitment Program of China and the National Key Research and Development Program of China (2016YFC0301202) to QPL, and the field work was a part of a Ph.D. dissertation by QPL. DAH was supported by U.S. National Science Foundation awards OCE-0241340 and OCE-0752972.

REFERENCES

Beckmann, A., and I. Hense. 2007. Beneath the surface: Characteristics of oceanic ecosystem under weak mixing conditions – a theoretical investigation. Prog. Oceanogr., *75*(4), 771–796. doi: 10.1016/j.pocean.2007.09.002

Bibby, T. S., M. Y. Gorbunov, K. W. Wyman, and P. G. Falkowski. 2008. Photosynthetic community responses to upwelling mesoscale eddies in the subtropical North Atlantic and Pacific Oceans. Deep Sea Res., Part II, *55*(10–13), 1310–1320. doi: 10.1016/j.dsr2.2008.01.014

Buesseler, K. O., C. Lamborg, P. Cai, R. Escoube, R. Johnson, S. Pike, P. Masque, D. McGillicuddy, and E. Verdeny. 2008. Particle fluxes associated with mesoscale eddies in the Sargasso Sea. Deep Sea Res., Part II, *55*(10–13), 1426–1444. doi: 10.1016/j.dsr2.2008.02.007

Calvo-Díaz, A., L. Díaz-Perez, L. A. Suárez, X. A. G. Morán, E. Teira, and E. Marañón. 2011. Decrease in the autotrophic-to-heterotrophic biomass ratio of picoplankton in oligotrophic marine waters due to bottle enclosure. Appl. Environ. Microbiol., *77*(16), 5739–5746. doi: 10.1128/AEM.00066-11

Cloern, J. E. 1999. The relative importance of light and nutrient limitation of phytoplankton growth: A simple index of coastal ecosystem sensitivity to nutrient enrichment. Aquat. Ecol., *33*(1), 3–16. doi: 10.1023/A:1009952125558

Cullen, J. J. 1982. The deep chlorophyll maximum: Comparing vertical profiles of chlorophyll *a*. Can. J. Fish. Aquat. Sci., *39*(5), 791–803. doi: 10.1139/f82-108

Cullen, J. J. 2015. Subsurface chlorophyll maximum layers: Enduring enigma or mystery solved? Annu. Rev. Mar. Sci., *7*, 207–239. doi: 10.1146/annurev-marine-010213-135111

Denaro, G., D. Valenti, B. Spagnolo, G. Basilone, S. Mazzola, S. W. Zgozi, S. Aronica, and A. Bonanno. 2013. Dynamics of two picophytoplankton groups in Mediterranean Sea: Analysis of the deep chlorophyll maximum by a stochastic advection-reaction-diffusion model. PLoS One, *8*(6), e66765. doi: 10.1371/journal.pone.0066765

Ewart, C. S., M. K. Meyers, E. R. Wallner, D. J. McGillicuddy Jr. and C. A. Carlson 2008. Microbial dynamics in cyclonic and anticyclonic modewater eddies in the northwestern Sargasso Sea Deep Sea Res., Part II, *55*(10–13), 1334–1347. doi: 10.1016/j.dsr2.2008.02.013

Fennel, K., and E. Boss. 2003. Subsurface maxima of phytoplankton and chlorophyll: Steady-state solutions from a simple model. Limnol. Oceanogr., *48*(4), 1521–1534. doi: 10.4319/lo.2003.48.4.1521

Gasol, J. M., P. A. del Giorgio, and C. M. Duarte. 1997. Biomass distribution in marine planktonic communities. Limnol. Oceanogr., *42*(6), 1353–1363. doi: 10.4319/lo.1997.42.6.1353

Geider, R. J., H. L. MacIntyre, and T. M. Kana. 1997. Dynamic model of phytoplankton growth and acclimation: Responses of the balanced growth rate and the chlorophyll *a*:carbon ratio to light, nutrient-limitation and temperature. Mar. Ecol. Prog. Ser., *148*, 187–200. doi: 10.3354/meps148187

Goericke, R., and N. A. Welschmeyer. 1998. Response of Sargasso Sea phytoplankton biomass, growth rates and primary production to seasonally varying physical forcing. J. Plankton Res., *20*(12), 2223–2249. doi: 10.1093/plankt/20.12.2223

Goldthwait, S. A. and D. K. Steinberg 2008. Elevated biomass of mesozooplankton and enhanced fecal pellet flux in cyclonic and modewater eddies in the Sargasso Sea. Deep Sea Res., Part II, *55*(10–13), 1360–1377 doi: 10.1016/j.dsr2.2008.01.003

Hodges, B. A., and D. L. Rudnick. 2004. Simple models of steady deep maxima in chlorophyll and biomass. Deep Sea Res, Part I,*51*(8), 999–1015. doi: 10.1016/j.dsr.2004.02.009

Huisman, J., N. N. Pham Thi, D. M. Karl, and B. Sommeijer. 2006. Reduced mixing generates oscillations and chaos in the oceanic deep chlorophyll maximum. Nature, *439*, 322–325. doi: 10.1038/nature04245

Ledwell, J. R., D. J. McGillicuddy Jr., and L. A. Anderson. 2008. Nutrient flux into an intense deep chlorophyll layer in a mode-water eddy. Deep Sea Res., Part II, *55*(10–13), 1139–1160. doi: 10.1016/j.dsr2.2008.02.005

Letelier, R. M., D. M. Karl, M. R. Abbott, and R. R. Bidigare. 2004. Light driven seasonal patterns of chlorophyll and nitrate in the lower euphotic zone of the North Pacific subtropical gyre. Limnol. Oceanogr., *49*(2), 508–519. doi: 10.4319/lo.2004.49.2.0508

Li, Q. P., P. J. S. Franks, M. R. Landry, R. Goericke, and A. G. Taylor. 2010. Modeling phytoplankton growth rates and chlorophyll to carbon ratios in California coastal and pelagic ecosystems. J. Geophys. Res.: Biogeosci., *115*, G04003. doi: 10.1029/2009jg001111

Li, Q. P., P. J. S. Franks, M. D. Ohman, and M. R. Landry. 2012. Enhanced nitrate fluxes and biological processes at a frontal zone in the southern California current system. J. Plankton Res., *34*(9), 790–801. doi: 10.1093/plankt/fbs006

Li, Q. P., and D. A. Hansell. 2008. Nutrient distributions in baroclinic eddies of the oligotrophic North Atlantic and inferred impacts on biology. Deep Sea Res., Part II, *55*(10–13), 1291–1299. doi: 10.1016/j.dsr2.2008.01.009

Li, Q. P., D. A. Hansell, D. J. McGillicuddy Jr., N. R. Bates, and R. J. Johnson. 2008. Tracer-based assessment of the origin and biogeochemical transformation of a cyclonic eddy in the Sargasso Sea. J. Geophys. Res.: Oceans, *113*, C10006. doi: 10.1029/2008jc004840

Li, Q. P., Y. Wang, Y. Dong, and J. Gan. 2015. Modeling the long-term change of planktonic ecosystems in the northern South China Sea and the upstream Kuroshio current. J. Geophys. Res.: Oceans, *120*(6), 3913–3936. doi: 10.1002/2014JC010609

Lipschultz, F. 2001. A time-series assessment of the nitrogen cycle at BATS. Deep Sea Res., Part II, *48*(8–9), 1897–1924. doi: 10.1016/S0967-0645(00)00168-5

Litchman, E. A. 2000. Growth rates of phytoplankton under fluctuating light. Freshwater Biol., *44*(2), 223–235. doi: 10.1046/j.1365-2427.2000.00559.x

Lomas, M. W., and F. Lipschultz. 2006. Forming the primary nitrite maximum: Nitrifiers or phytoplankton? Limnol. Oceanogr., *51*(5), 2453–2467. doi: 10.4319/lo.2006.51.5.2453

Mackey, K. R. M., A. Paytan, A. R. Grossman, and S. Bailey. 2008. A photosynthetic strategy for coping in a high-light, low-nutrient environment. Limnol. Oceanogr., *53*(3), 900–913. doi: 10.4319/lo.2008.53.3.0900

McGillicuddy, D. J., Jr., L. A. Anderson, N. R. Bates, T. Bibby, K. O Buesseler, C. A. Carlson, C. S. Davis, et al. 2007. Eddy/wind interactions stimulate extraordinary mid-ocean plankton blooms. Science, *316*(5827), 1021–1026. doi: 10.1126/science.1136256

Probyn, T. A., B. A. Mitchell-Innes, and S. Searson. 1995. Primary productivity and nitrogen uptake in the subsurface chlorophyll maximum on the eastern Agulhas Bank. Cont. Shelf Res., *15*(15), 1903–1920. doi: 10.1016/0278-4343(94)00099-9

Riegman, R. 1998. Species composition of harmful algal blooms in relation to macronutrient dynamics, *in* Physiological Ecology of Harmful Algal Blooms, D. M. Anderson, A. D. Cembella, and G. M. Hallegraeff, eds. Berlin: Springer Verlag, 489–508.

Shampine, L. F., and M. W. Reichelt. 1997. The MATLAB ODE suite. SIAM J. Sci. Comput., *18*(1), 1–22. doi: 10.1137/S1064827594276424

Siegel, D. A., A. F. Michaels, J. C. Sorensen, M. C. O'Brien, and M. A. Hammer. 1995. Seasonal variability of light availability and utilization in the Sargasso Sea. J. Geophys. Res.: Oceans, *100*(C5), 8695–8713. doi: 10.1029/95JC00447

Siegel, D. A., T. K. Westberry, M. C. O'Brien, N. B. Nelson, A. F. Michaels, J. R. Morrison, A. Scott, et al. 2001. Bio-optical modeling of primary production on regional scales: The Bermuda BioOptics project. Deep Sea Res., Part II, *48*(8–9), 1865–1896. doi: 10.1016/S0967-0645(00)00167-3

Strass, V. H. 1992. Chlorophyll patchiness caused by mesoscale upwelling at fronts. Deep-Sea Res., Part A, *39*(1), 75–96. doi: 10.1016/0198-0149(92)90021-K

Villareal, T. A., C. Pilskaln, M. Brzezinski, F. Lipschultz, M. Dennett, and G. B. Gardner. 1999. Upward transport of oceanic nitrate by migrating diatom mats. Nature, *397*, 423–425. doi: 10.1038/17103

Weston, K., L. Fernand, D. K. Mills, R. Delahunty, and J. Brown. 2005. Primary production in the deep chlorophyll maximum of the central North Sea. J. Plankton Res., *27*(9), 909–922. doi: 10.1093/plankt/fbi064

Received: *21 September 2015*; revised: *22 June 2016*.